Supporting Information

Defects in Nanosilica Catalytically Convert CO_2 to Methane without Any Metal and Ligand

Amit K. Mishra,[1] Rajesh Belgamwar,[1] Rajkumar Jana,[2] Ayan Datta,[2] and Vivek Polshettiwar[1]*
[1]Department of Chemical Sciences, Tata Institute of Fundamental Research (TIFR), Mumbai, India.
[2]School of Chemical Sciences, Indian Association for the Cultivation of Science, Jadavpur, Kolkata, India
Email: vivekpol@tifr.res.in,

Experimental Details

Synthesis of defect-containing nanosilica using the magnesiothermic protocol.

In a typical synthesis, 250 mg DFNS and 10, 25 and 50 wt. % Mg powder was mixed well with a mortar and pestle. The whitish-grey powder was then transferred to a tubular quartz tube, which was degassed overnight to remove atmospheric oxygen. The tube was then sealed under vacuum and heated in a furnace to 675 °C at a rate of 5 °C min^{-1} and then held at this temperature for 12 h. The grey powder (defect-containing nanosilica and MgO) was collected by breaking the tube. The samples were then stirred with an acidic solution (6.8 mL HCl 12M, 17 mL H_2O, and 52 mL ethanol) for 24 h at room temperature to dissolve the MgO. The solid product was isolated by centrifugation. This step was repeated three times, and after that samples were washed by 40 mL each of water and ethanol twice. Washing was continued until all Mg containing species such as Mg_2SiO_4, MgO and Mg are completely absent from the defect-containing silica, which was monitored by EDS elemental analysis and their absence was further confirmed by PXRD and XPS. The samples were dried in an oven overnight and the defect-containing nanosilica powder was stored under atmospheric conditions.

Characterization. Scanning transmission electron microscope (STEM) analysis was carried out on FEI-TITAN operated at an accelerating voltage of 300 kV. The samples were prepared by dispersing a small amount of powder in ethanol by sonication and dropping the solution on a 200 mesh carbon-coated TEM grid. Elemental analysis was achieved using the energy-dispersive X-ray spectroscopy (EDS). A Panalytical X'Pert Pro powder X-ray diffractometer was used to record X-ray diffraction patterns using a Cu *Kα* source. The surface area, pore-volume, and pore size distribution measurements were carried out using Micromeritics Flex-3 analyzer by applying BET theory to the N_2 physisorption data. Before analysis, all samples were degassed at 120 °C for 12

www.pnas.org/cgi/doi/10.1073/pnas.1917237117

h. A UV/vis/NIR spectrophotometer was used to record the UV-visible diffuse reflectance spectra (UV-DRS) of all samples. The FTIR spectra were recorded using JASCO FT/IR-4700. The EPR spectra of all samples were recorded at room temperature using JEOL EPR spectrometer. Following conditions were used to record EPR spectra of the catalyst, amount = 30 mg, power = 5 mW, modulation frequency =100 kHz, number of scans = 5. XPS measurements were carried out using Thermo $K\alpha$+ spectrometer using micro-focused and monochromated Al-K_α radiation with an energy of 1486.6 eV. Charge correction of all spectra was achieved by fixing the energy of the C1s peak at 284.5 eV. All fitting was done in XPSPEAK 4.1 by taking Taugaard background. For the PL measurements, excitation was carried out at 374 nm using a diode laser, with the sample placed in the integrating sphere. For the DRIFT study, the IR spectra were recorded using a mixture of 3.5 mg catalyst and 156 mg KBr powder in a closed reactor chamber, with a heater and gas flow controller. The catalyst was activated at 550 °C with 50 mL min^{-1} air before the measurements. After cooling to the desired temperature, the feed gases (2.5 mL CO_2 and 10 mL H_2) were passed through the chamber, and IR spectra were recorded over time under different reaction conditions.

Catalytic CO_2 conversion. The methanation reaction was carried out in a fixed-bed continuous flow reactor (PIDengtech). 200 mg of catalyst was placed in a tubular reactor (of diameter 0.9 cm and length 12 cm). The reactor was heated to 550 °C at a rate of 20 °C min^{-1} with 50 mL min^{-1} flow of air to remove atmospheric carbon contamination. After cooling the reactor to 400 °C in the presence of air and N_2, the reactive gases were fed (2.5 mL min^{-1} CO_2, 10 mL min^{-1} H_2 and 2.5 mL min^{-1} N_2 as an internal standard) by mass flow controllers (MFC) for individual gases. The reaction progress and product quantification was achieved by gas chromatography (GC, Agilent 7890 B) with a flame ionization detector (FID) and thermal conductivity detector (TCD), using an Agilent hybrid column CP7430 to separate the CO_2, CH_4 and CO. Peltier cooling was used to condense and collect the water by-product from the reactor.

Using standard calibration gases, we calculated the methane and CO production in ppm, using peak area of methane and CO in GC.

$$\text{Production rate of CH4 } (\mu\text{mol g}^{-1}\text{ h}^{-1}) = \frac{CH4\ (in\ ppm/mL) \times outlet\ flow\ (mL/min) \times 60}{22400 \times weight\ of\ the\ catalyst\ in\ gm}$$

$$\text{Production rate of CO } (\mu\text{mol g}^{-1}\text{ h}^{-1}) = \frac{CO\ (in\ ppm/mL) \times outlet\ flow\ \ (mL/min) \times 60}{22400 \times weight\ of\ the\ catalyst\ in\ gm}$$

Carbon balance for DNS-25 Catalytic Process

CO_2 flow (inlet) = 2.5 mL/min

CO_2 Conversion = 13 %,

CO_2 Converted = 0.325 mL/min

= 14.5 μmol/ min

Reaction Time (h)	**CH_4 (μmol/min)**	**CO (μmol/min)**	**Carbon balance (μmol/min)**
0.5	9.4	5.2	14.6
1	9.3	5.3	14.6
1.5	9.2	5.4	14.6
2	8.9	5.5	14.4
2.5	8.9	5.6	14.5
3	8.9	5.4	14.3

Reproducibility Check: The defect-containing silica was synthesized for more than ten times and the success rate was 90%. The 10% failure rate was due to the improper degassing of the quartz tube or improper mixing of DFNS and Mg. Catalysis was reproduced three times and regeneration experimenters were carried out four times.

Computational Details: All the spin-polarized calculations were performed within the framework of density functional theory (DFT) using the plane-wave technique as implemented in Vienna Ab Initio Simulation Package (VASP).[1] The exchange-correlation energy was accounted within the generalized gradient approximation method (GGA) parameterized by the Perdew-Burke-Ernzerhof (PBE).[2] We used the projector augmented wave potential (PAW) to treat the ion-electron interactions. The DFT-D2 empirical correction method proposed by Grimme was applied for describing the effect of van der Waals interactions.[3] In all computations, the kinetic energy cut off is set to be 500 eV in the plane-wave expansion. All the structures were fully relaxed (lattice constant and atomic position) using the conjugated gradient method and the convergence threshold was set to be 10^{-4} eV in energy and 0.01 eV/Å in force. For geometry optimization, the Brillouin zone was sampled using a 5×5×1 Monkhorst-Pack k-point mesh. In order to calculate the charge transfer between the CO_2 molecule and amorphous nanosilica (DFNS) surface slab, we chose

Bader charge-population analysis method.[4,5] For structure optimization of the CO_2 molecule in gas phase we used B3LYP/6-31+G (d,p) method as implemented in Gaussian 09.[6] The climbing image nudge elastic band method (CI-NEB) was used to calculate activation barriers and six intermediate images were considered along the minimum energy path (MEP) to search for transition states for the intermediate states toward CO_2 reduction.[7] For all the pathways, the activation barriers ($\Delta E^{\ddagger}$) were calculated using the following equations: $\Delta E^{\ddagger} = E_{TS} - E_{IS}$ and $\Delta E = E_{FS} - E_{IS}$; where IS, TS and FS correspond to initial state, transition state, and final state, respectively. The adsorption energy (E_{ad}) of adsorbates i.e. intermediate molecules and /or atoms on silica surface was defined as:

$$E_{ad} = E_{A/S} - E_A - E_S$$

Where $E_{A/S}$, E_A and E_S represents total energies of the surface slab with adsorbates, only adsorbates and DFNS surface

The reaction energy (E_r) was calculated using the following equation[8]

$$E_r = E_{FS} - E_{IS}$$

In order to model DFNS surface with various types of the defect (i.e. ODC, NBOHC and E' centres), we considered a periodic surface slab with 14.35 × 7.18 $Å^2$ rectangular surface cell with 53 atoms. To avoid the spurious interactions between the neighbouring slabs, a vacuum layer of 20 Å is used in the direction perpendicular to the surfaces (along Z-direction) and the nearest distance between the two adsorbed molecules in the adjacent supercell is ~8 Å.

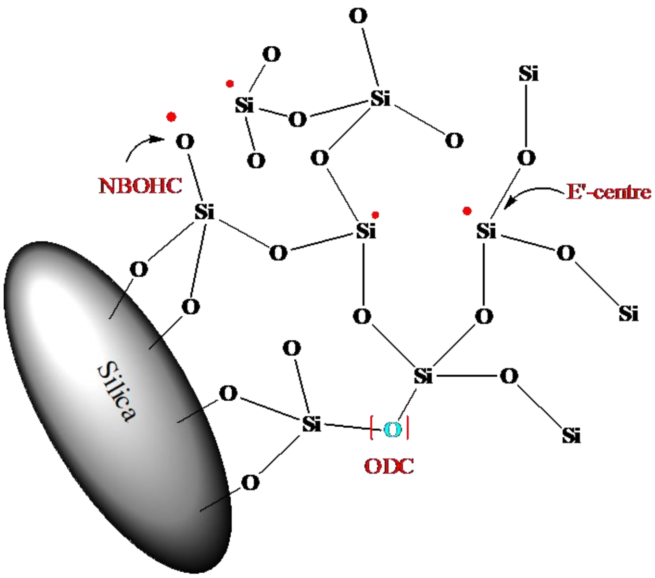

Figure S1. Schematic representation of the defects in amorphous silica, E'-centres, ODCs and NBOHCs.

(A)

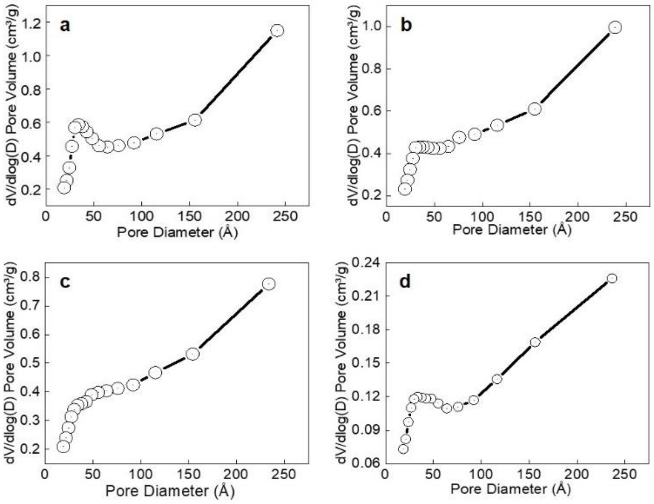

(B)

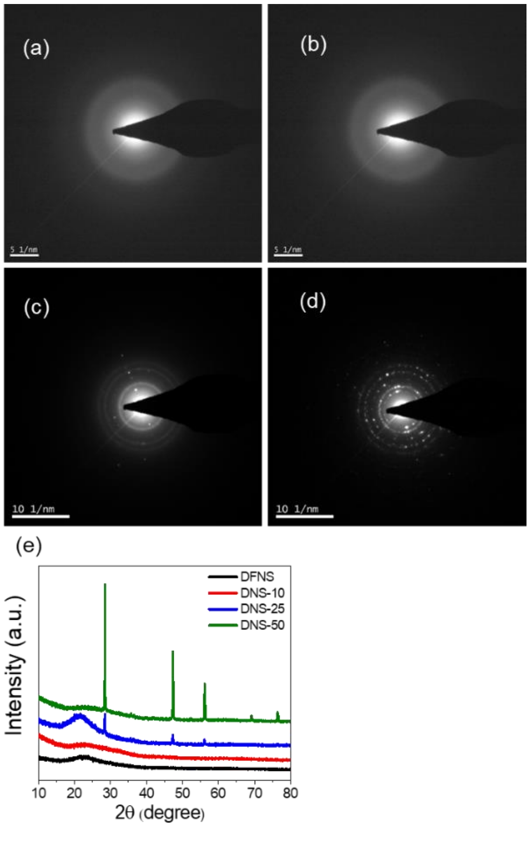

Figure S2. (A) **The Barrett–Joyner–Halenda (BJH) adsorption pore size distribution** indicates the existence of the two different types of pores, one having a narrow distribution between 20 and 60 Å and one having a broad distribution between 60 and 250 Å; (B) **Selective area electron diffraction (SAED) and PXRD of various defect-containing nanosilica, (**a) DFNS, (b) DNS-10, (c) DNS-25 and (d) DNS-50, indicated that defect-containing silica is still amorphous in nature. However, a small percentage of crystalline silicon was observed in the case of DNS-25, whose XRD pattern contains diffraction peaks at 28.4°, 47.6°, 56.4°, 69.6°, and 76.4°, and more crystalline silicon concentration was observed in DNS-50.

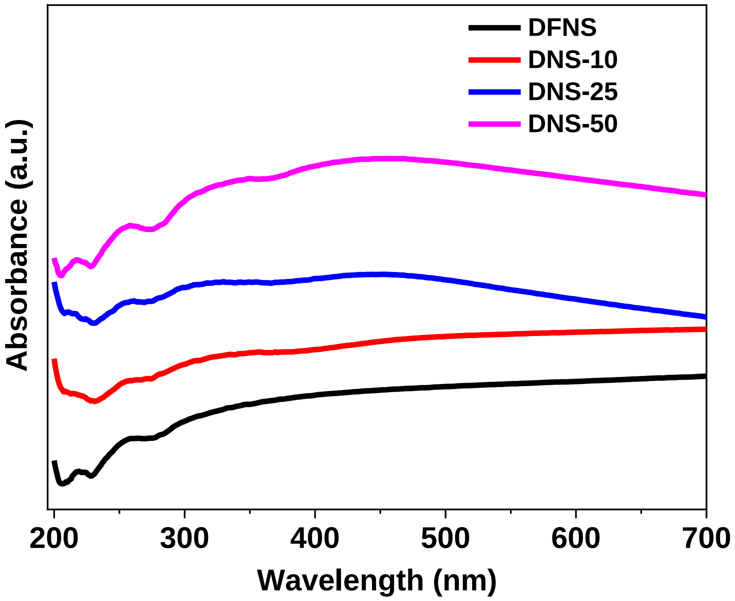

Figure S3. UV-DRS spectra of defect-containing nanosilicas. Band at 209 and 216 nm for surface and bulk E'-centres respectively.[27] The bands at 258 and 284 nm were assigned to bulk and surface NBOHCs, respectively, corresponding to charge transfer from a 2p non-bonding orbital of the oxygen connected to Si-O• to a 2p non-bonding orbital of non-bridging oxygen, ($O_3Si\text{-}O \rightarrow (O_3^+Si\text{-}O{\bullet\bullet})^*$). The band at 336 nm was assigned to bulk peroxy radicals formed because of the strong adsorption of oxygen to the E'-centres (≡Si-O–O·). The broadband at approximately 525 nm was also assigned to the ODC present in the silica framework.[27]

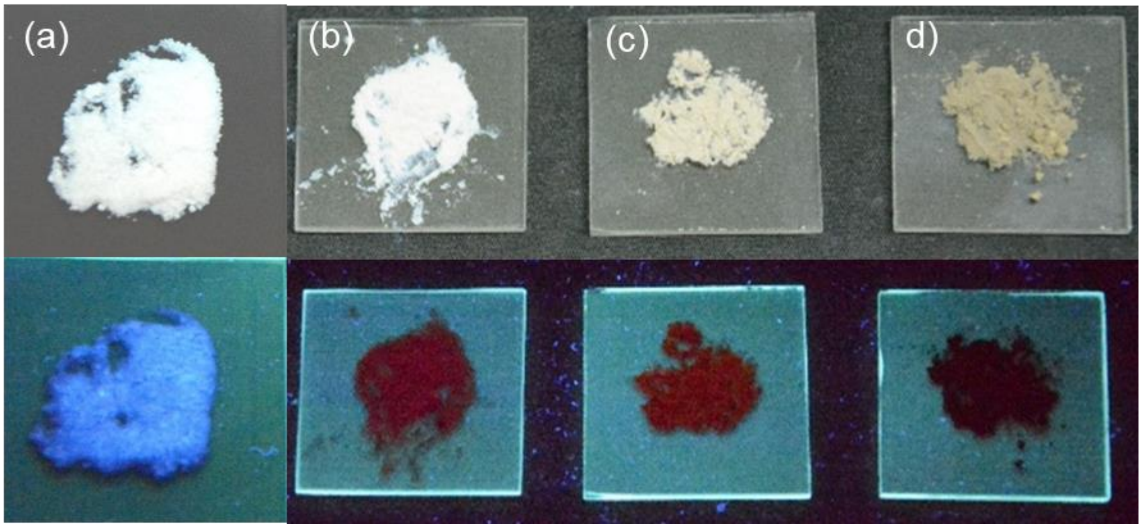

Figure S4. Photographic images of (a) DFNS, (b) DNS-10, (c) DNS- 25, and (d) DNS-50, under normal light (top) and UV light (bottom).

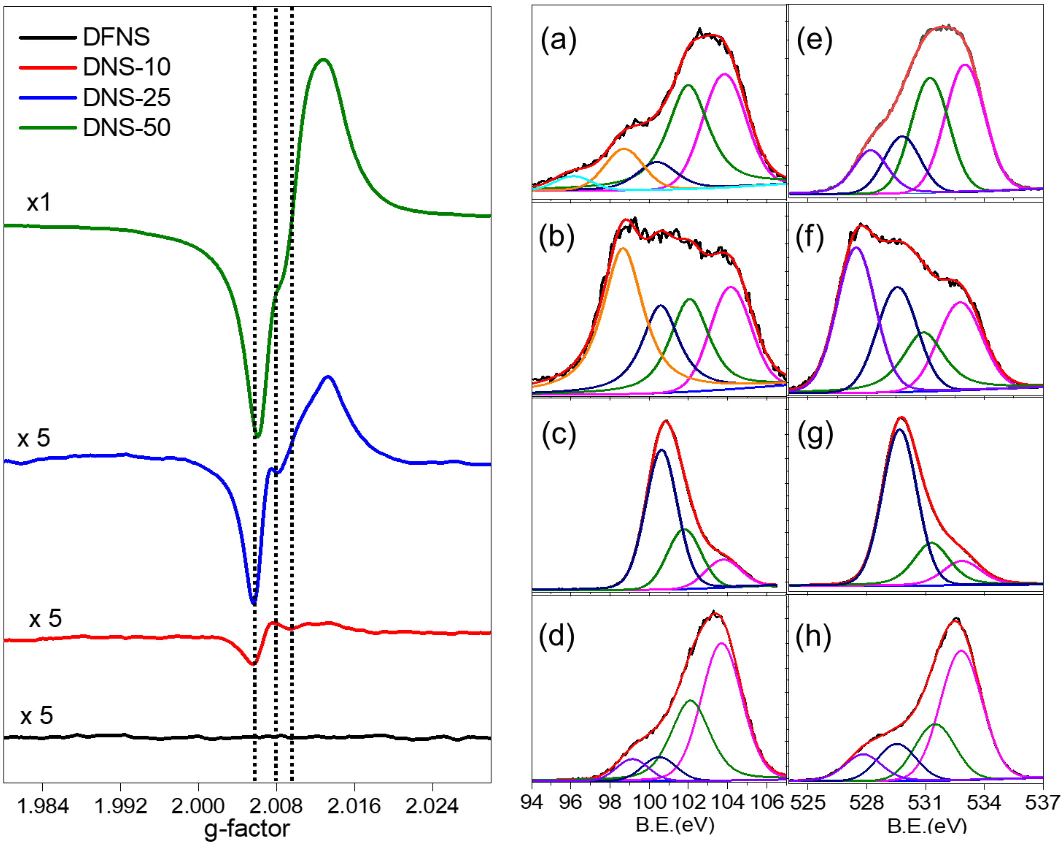

Figure S5. (Left panel) EPR spectra of various defect-containing nanosilica. (Right panel) XPS spectra for Si (2p) core levels of (a) DFNS, (b) DNS-10, (c) DNS-25, (d) DNS-50, and XPS spectra for the O (1s) core levels of (e) DFNS, (f) DNS-10, (g) DNS-25, (h) DNS-50.

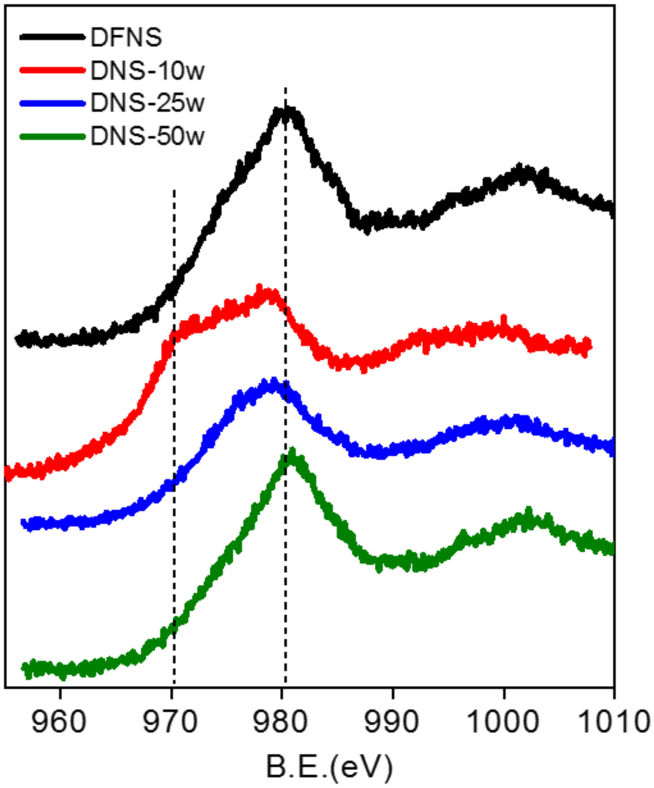

Figure S6. Auger spectra of defect-containing nanosilicas.

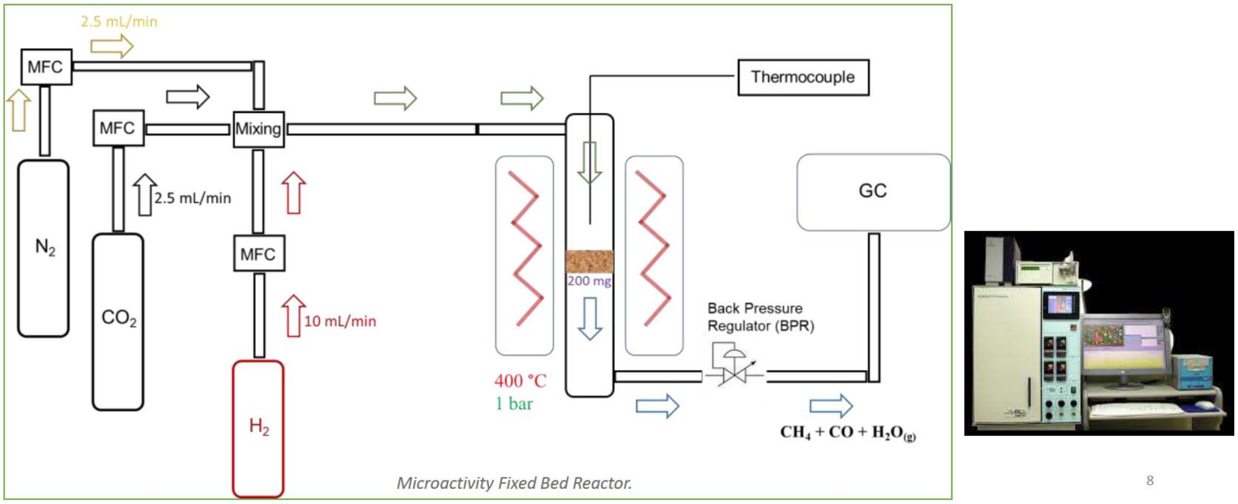

Figure S7. Reactor set-up for CO_2 methanation using a fixed-bed micro activity reactor under flow conditions**.**

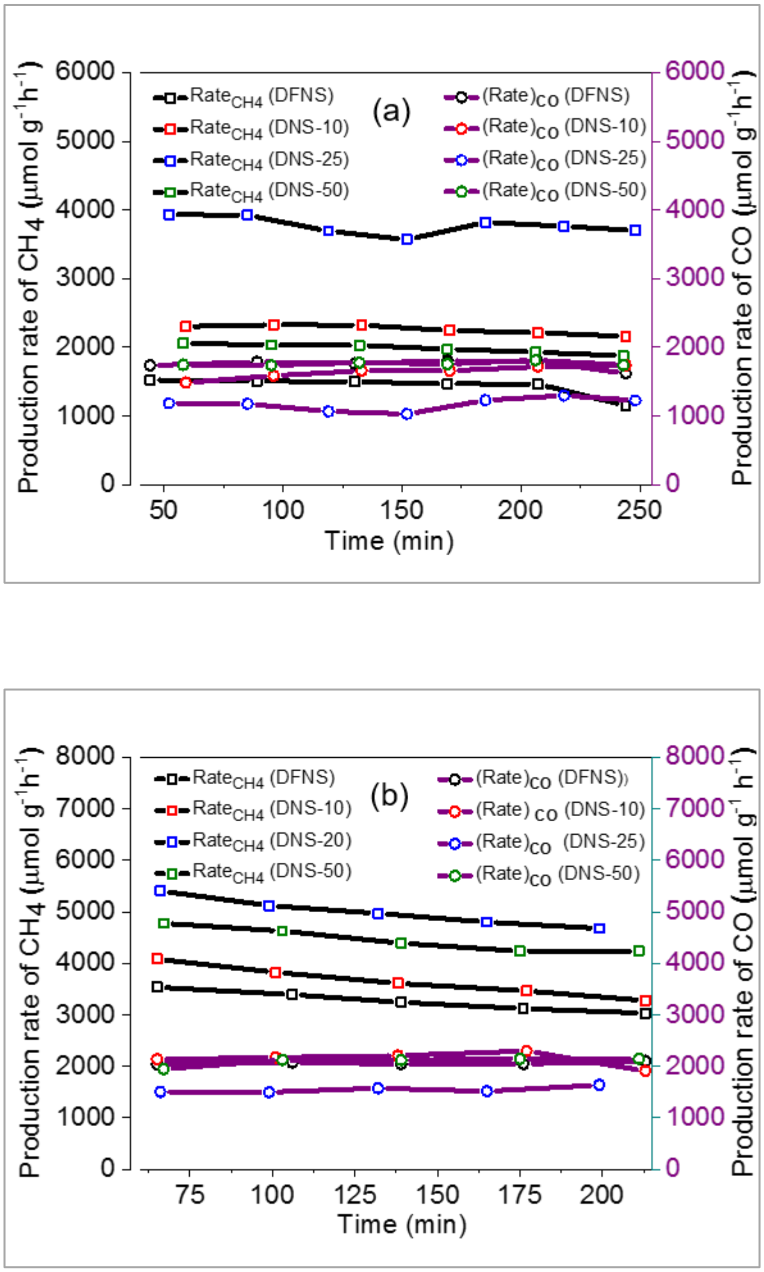

Figure S8. Reaction progress with time for rate of methane and CO production (a) at 400 °C and 1 bar, (b) 400 °C and 10 bar.

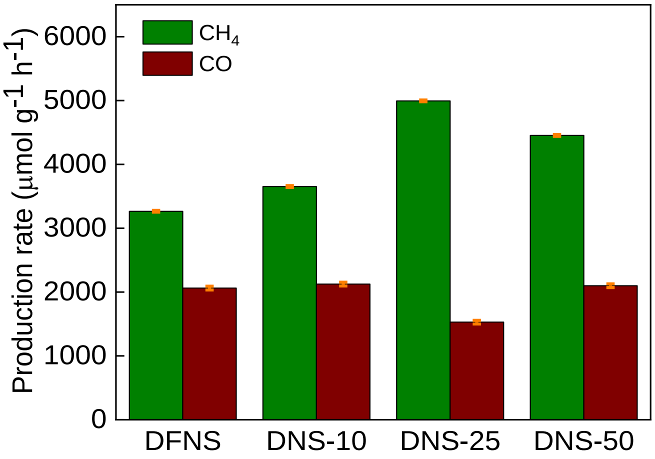

Figure S9. Production rates of CH_4 and CO for various catalysts at 400 °C and 10 bar.

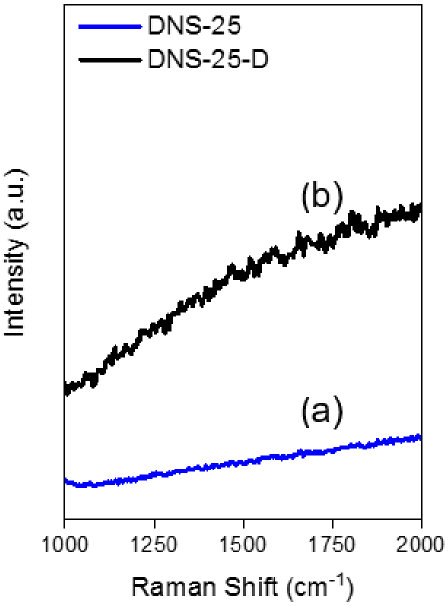

Figure S10. Raman spectra of defect-containing nanosilica (a) before (DNS-25) and (b) after (DNS-25-D) catalysis.

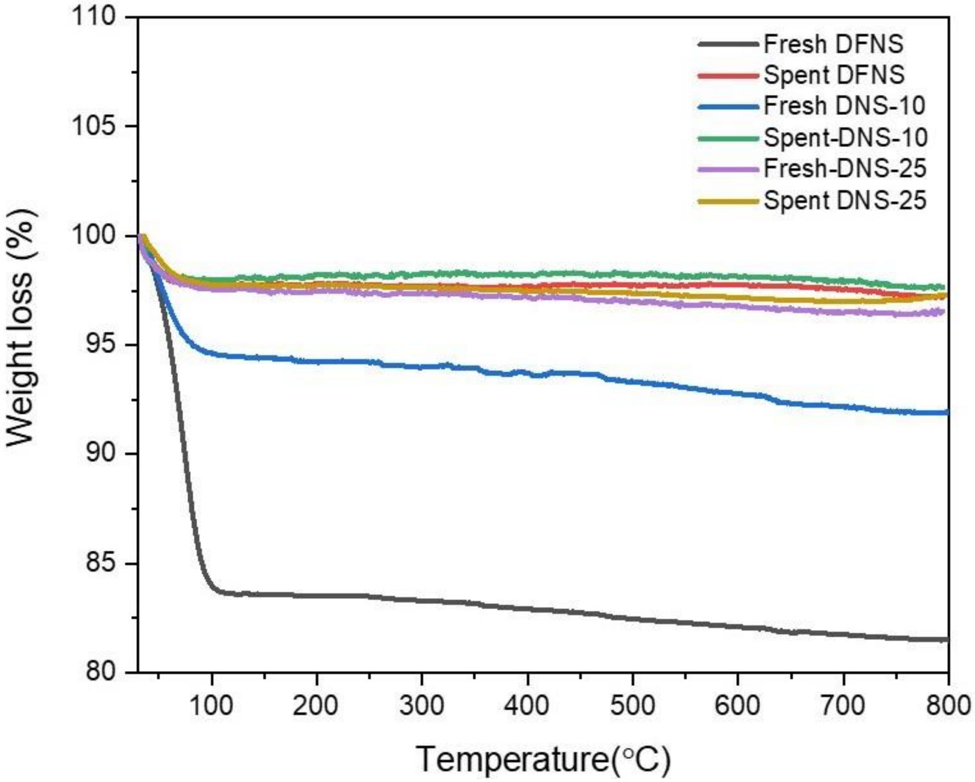

Figure S11. Temperature-programmed oxidation of fresh and spent catalysts in TGA

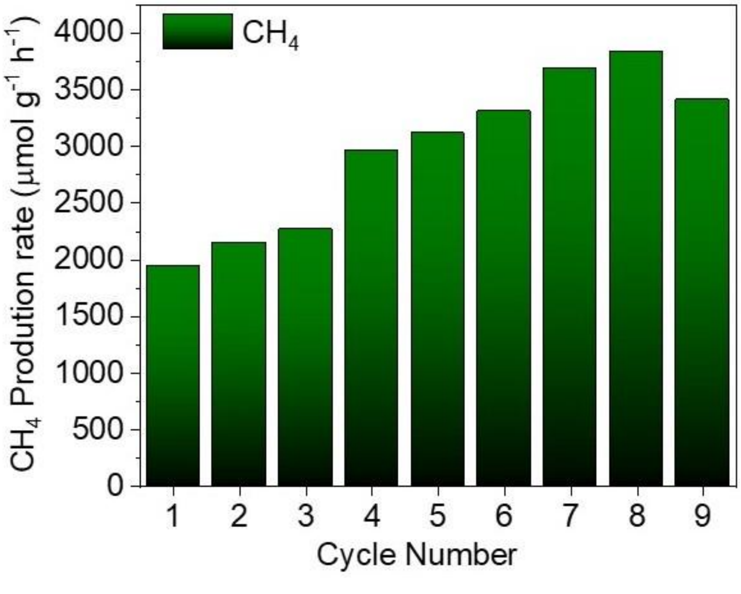

Figure S12. Regeneration of catalysts DNS-10 in air at 400 °C and 1 bar up to 9 cycles.

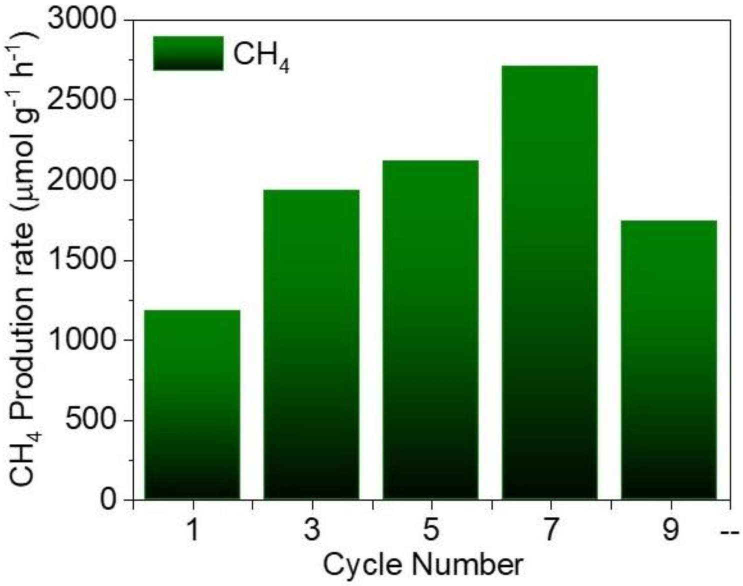

Figure S13. Regeneration of catalysts DFNS in air at 400 °C and 1 bar up to 9 cycles.

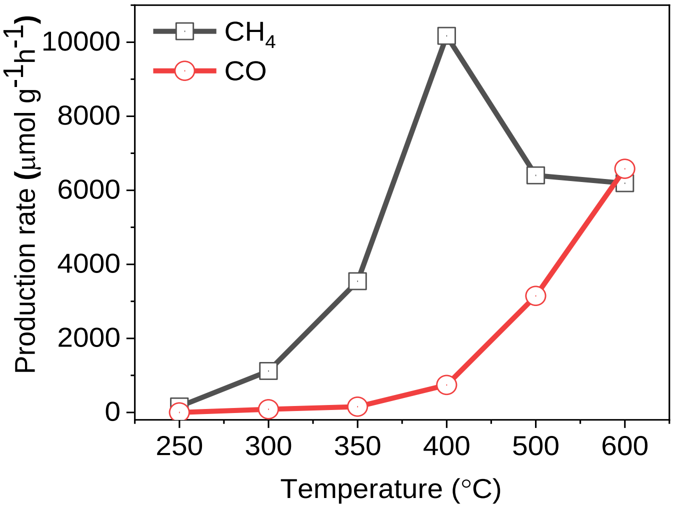

Figure S14. Temperature-dependent production rates of CH$_4$ and CO with the activated DNS-25 catalyst. The formation of methane started at 250 °C but with a poor rate, and the rate reached its maximum value at 400 °C. At higher temperatures (> 400 °C), the reverse water-gas shift reaction was favoured, as a result, the formation of methane decreased and the formation of CO increased.

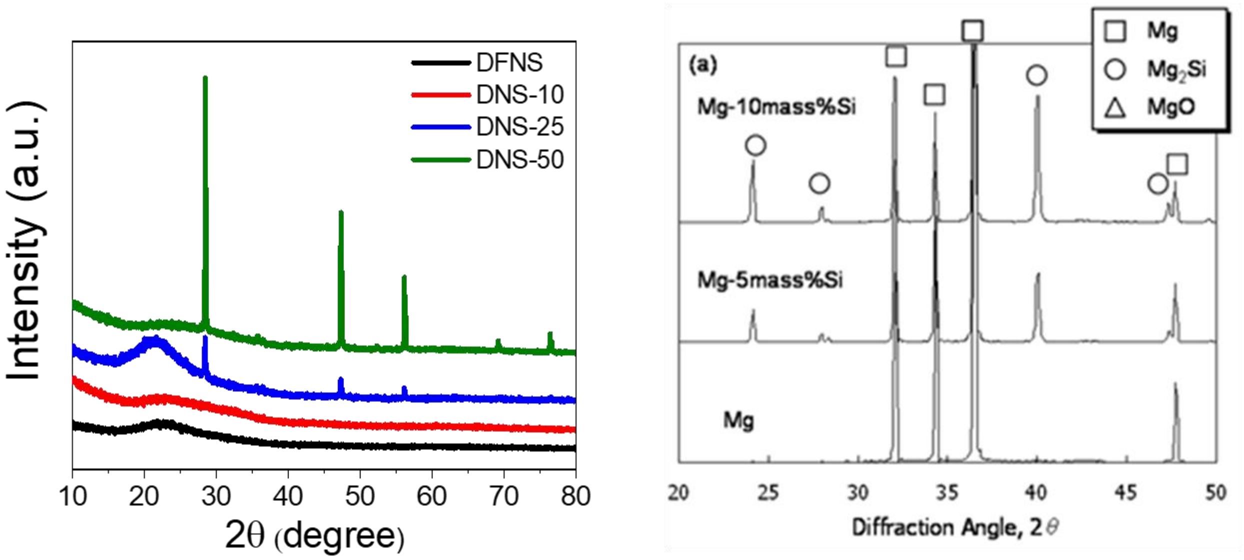

Ref. Katsuyoshi Kondoh, Ritsuko Tsuzuki and Eiji Yuasa,
DOI : 10.2240/azojomo0110

Figure S15. PXRD of DFNS, DNS-10, DNS- 25, DNS-50 (left panel) and their comparison with reported PXRD pattern for Mg, Mg_2Si and MgO (right panel).

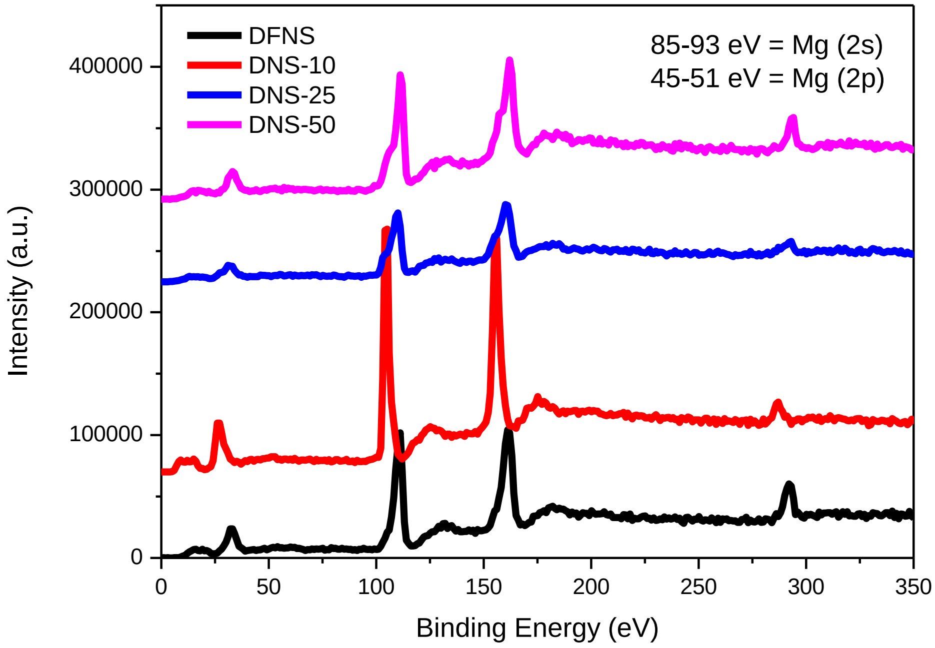

Figure S16. XPS spectra for DFNS, DNS-10, DNS- 25, DNS-50. . Mg, MgO, or Mg_2Si were reported to show XPS signals between 85-93 eV and 45-51 eV for Mg (2s) and Mg (2p), respectively. These signals were absent in all defect-containing silica confirming the purity of defect-containing silica.

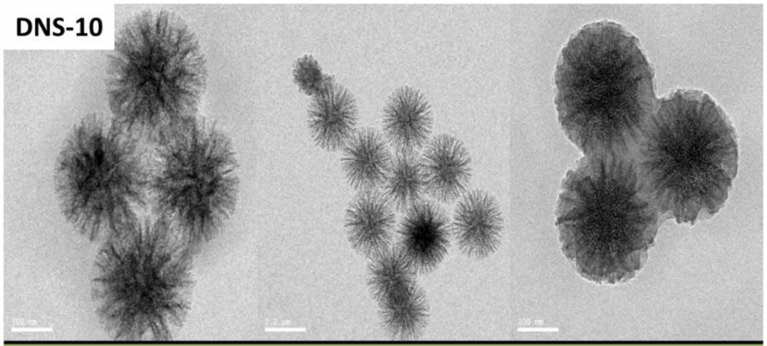

Element	Weight (%)	Atomic (%)	Error (%)
O (K)	63.10	74.96	0.47
Mg (K)	0.64	0.50	0.05
Si (K)	36.24	24.53	0.24

Figure S17. TEM images (top panel) and EDX elemental analysis (bottom) of DNS-10.

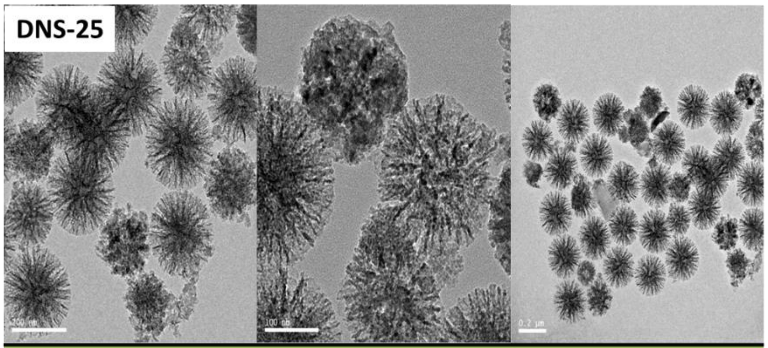

Element	Weight (%)	Atomic (%)	Error (%)
O (K)	55.40	68.56	0.27
Mg (K)	0.00	0.00	0
Si (K)	44.59	31.43	0.15

Figure S18. TEM images (top panel) and EDX elemental analysis (bottom) of DNS-25.

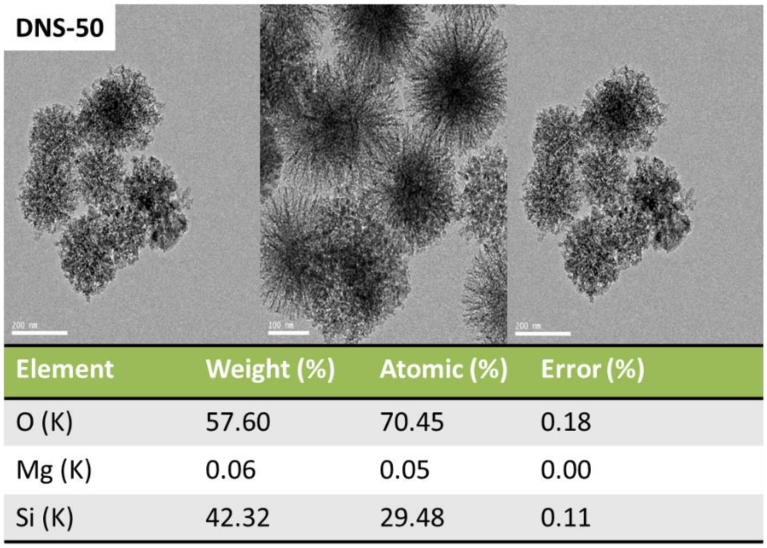

Element	Weight (%)	Atomic (%)	Error (%)
O (K)	57.60	70.45	0.18
Mg (K)	0.06	0.05	0.00
Si (K)	42.32	29.48	0.11

Figure S19. TEM images (top panel) and EDX elemental analysis (bottom) of DNS-50.

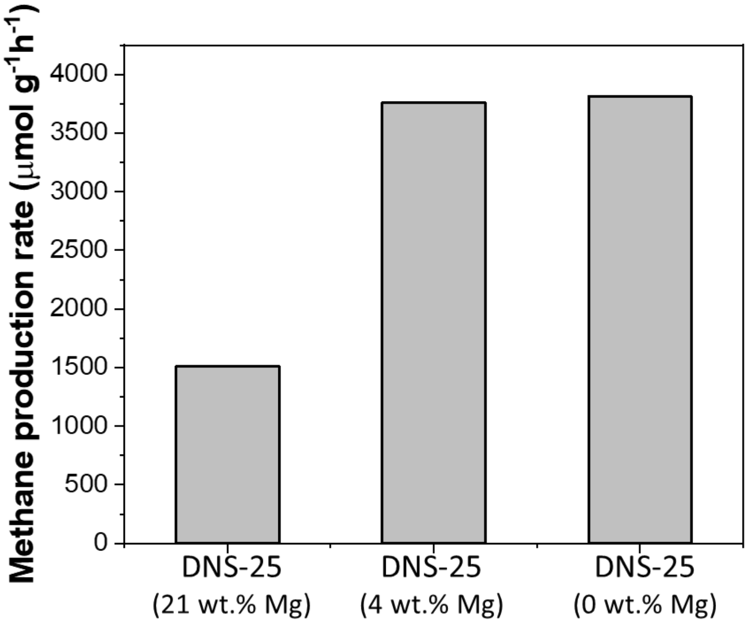

Figure S20. Production rates of CH_4 using DNS-25 with various Mg concentration at 400 °C and 1 bar.

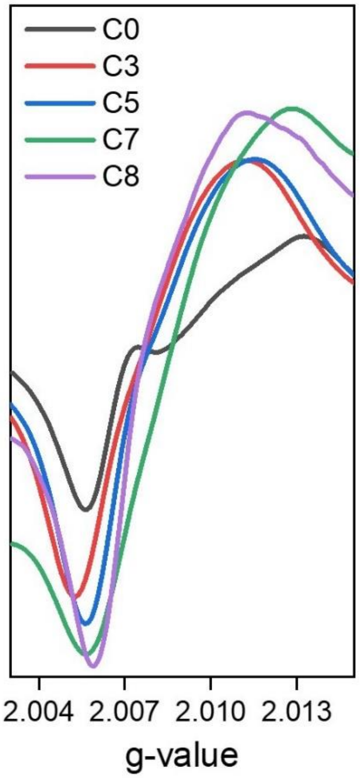

Figure S21. EPR of DNS-25 after various cycles (0, 3, 5, 7 & 8) of regeneration.

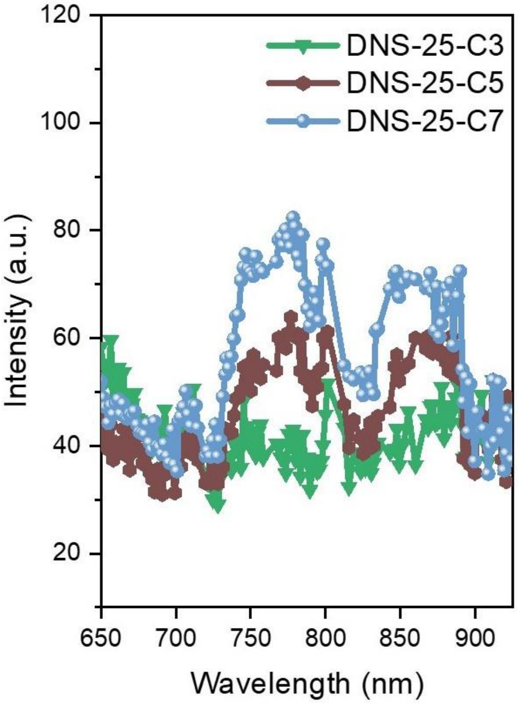

Figure S22. PL of DNS-25 after various cycles(3, 5 & 7) of regeneration**.**

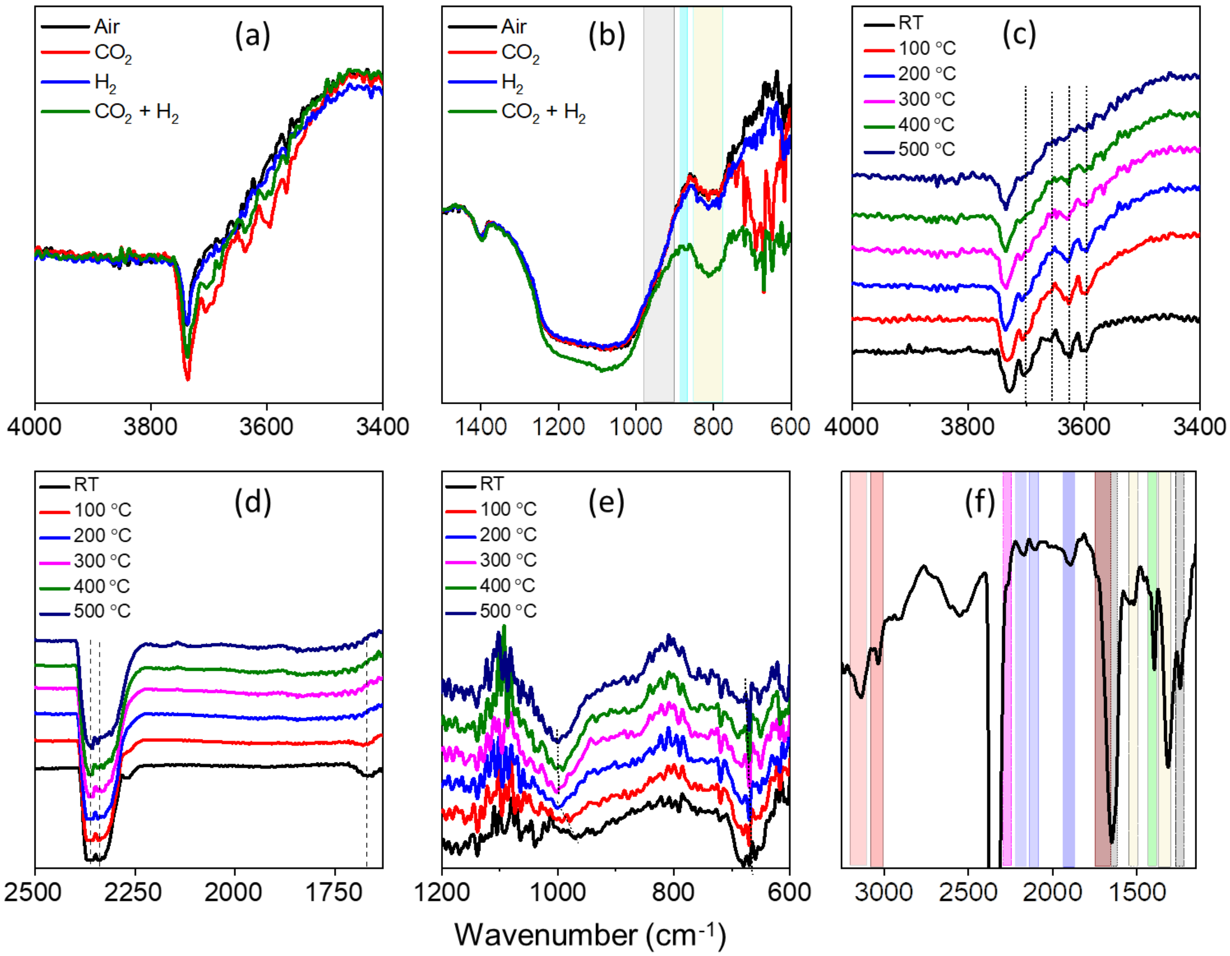

Figure S23. The effect on DNS-25 silanol stretching signals by gaseous (a) CO_2, H_2, and CO_2 + H_2 at 400 °C and 1 bar; (b) effect on Si-O-Si region, by CO_2, H_2 and CO_2 + H_2 at 400 °C and 1 bar; (c) IR signals of silanols during reaction at different temperatures in the presence of CO_2 + H_2 at 400 °C and 1 bar; (d) CO_2 adsorption during reaction at different temperatures in the presence of CO_2 + H_2; (e) IR spectra of gaseous CO_2 and formed bidentate carbonate at different temperatures in the presence of CO_2 + H_2; (f) IR spectra after instant cooling of the DRIFT chamber to room temperature.

When the gases (CO_2 and H_2) were individually fed over the catalyst, we found that IR peak at 3739 cm^{-1} for Si-OH stretching did not change after H_2 feeding (Figure S23a). In contrast, CO_2 feeding resulted in changes in the Si-OH peaks, which suggested that CO_2 gas is interacting with silanols. The peak in the 1260–1000 cm^{-1} region was assigned to the asymmetric stretching of Si-O-Si bonds, whereas the broad peak with a peak maximum at 1088 cm^{-1} was assigned to the TO_1 (transverse optical resonant mode) and the peak with a shoulder at 1200 cm^{-1} was assigned to the TO_2 mode (Figure S23b)[34,35].The peak at 1265 cm^{-1} was assigned to the LO_1 (longitudinal optical mode) of Si-O-Si whereas the peak at 1170 cm^{-1} was assigned to the LO_2 mode[34.] The symmetric stretching of the Si-O-Si bond was reported in 1200–850 cm^{-1} region whereas the broad peak at 900–980 cm^{-1} is characteristic of the Si-O symmetric stretching of the silanol group.[33,36] The band at 876–885 cm^{-1} corresponds to Si-H species (azure colour). [33,36] The temperature-dependent DRIFT measurements suggest that the intensity of peaks of adsorbed CO_2 was increased up to 400 °C but decreased at 500 °C (Figure S23d,). This suggests that silanol aids the adsorption of CO_2 at 400 °C whereas at 500 °C, the adsorbed CO_2 was desorbed.

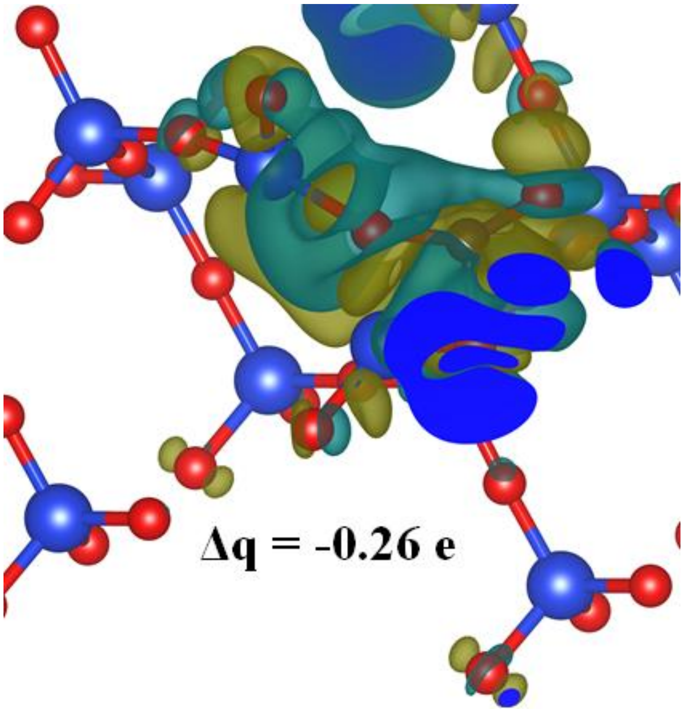

Figure S24. Charge density difference (CDD) plot (isodensity value at surfaces is ±0.002 e/au^3 (Positive: cyan and Negative: olive)) of CO_2 adsorbed a-SiO_2 surface showing charge transfer in the region between CO_2 and surface atoms upon adsorption of CO_2.

Table S1. Quantification of oxygen and silicon in defect-containing nanosilica from XPS data

The quantitative analysis further suggests that the surface of DFNS contains 53% bridging oxygen of siloxane, 22% silanol, and 14% NBHOC sites (Table S1). The XPS study showed that after magnesiothermic treatment, most of the siloxanes and silanol groups were converted to NBOHCs (61%) in DNS-10. As evident in the Si (2p) and O (1s) XPS spectra, there is a huge decrease in the concentration of NBOHCs from 61% in DNS-10 to 21% in DNS-25, which was also supported by EPR and PL measurements. The concentrations of silanol and siloxane Si and O were same in both samples (Table S1), suggesting that most of the NBOHCs were converted into E'-centres which were then converted into peroxy radicals because of adsorption of atmospheric O_2 at the E'-centres[27]. The analysis of the XPS spectrum of DNS-50 suggests the presence of 34% siloxane oxygen and about 41% silanol. The peak area related to NBOHCs decreased compared to that of DNS-25, while those of oxygen and silanol increased. This could be due to the oxidation of some surface silicon nanoparticles because of contact with atmospheric oxygen[28].

DFNS	**O (1s)**	**Si (2p)**
Siloxane	53 %	53 %
Silanol	34.2 %	22 %
NBOHC	14 %	7 %
E' or peroxy	6 % (peroxy)	11 % (E')
DNS-10		
Siloxane	12 %	13 %
Silanol	22 %	26 %
NBOHC	66 %	61 %
E' or peroxy	0 % (peroxy)	0 % (E')
DNS-25		
Siloxane	22 %	19 %
Silanol	19 %	21 %
NBOHC	25 %	21 %
E' or peroxy	34 % (peroxy)	34 % (E')
DNS-50		
Siloxane	38 %	34 %
Silanol	33 %	41 %
NBOHC	16 %	9 %
E' or peroxy	13 % (peroxy)	12 % (E' or Si)

References:

(1) Kresse, G.; Hafner, J. Ab initio molecular dynamics for liquid metals. *Phys. Rev. B* **1993,** *47*, 558.

(2) Perdew, J. P.; Burke, K.; Ernzerhof, M. Generalized gradient approximation made simple. *Phys. Rev. Lett.* **1996,** *77*, 3865.

(3) Grimme, S. Semiempirical GGA-type density functional constructed with a long-range dispersion correction. *J. Comput. Chem.* **2006,** *27*, 1787-1799.

(4) Henkelman, G.; Arnaldsson, A.; Jónsson, H. A fast and robust algorithm for Bader decomposition of charge density. *Comput. Mater. Sci.* **2006,** *36*, 354-360.

(5) R. F. W. Bader, "Atoms in Molecules: A Quantum Theory," Oxford University Press, Oxford, **1990**.

(6) Gaussian09, R. A. 1, Frisch, M. J., Trucks, G. W., Schlegel, H. B., Scuseria, G. E., Robb, M. A., Cheeseman, J. R., Scalmani, G., Barone, V., Mennucci, B., Petersson, G. A., Nakatsuji, H., Caricato, M., Li, X., Hratchian, H. P., Izmaylov, A. F., Bloino, J., Zheng, G., Sonnenberg, J. L., Hada, M., Ehara, M., Toyota, K., Fukuda, R., Hasegawa, J., Ishida, M., Nakajima, T., Honda, Y., Kitao, O., Nakai, H., Vreven, T., Montgomery, J. A., Jr., Peralta, J. E., Ogliaro, F., Bearpark, M., Heyd, J. J., Brothers, E., Kudin, K. N., Staroverov, V. N., Kobayashi, R., Normand, J., Raghavachari, K., Rendell, A., Burant, J. C., Iyengar,S. S., Tomasi, J., Cossi, M., Rega, N., Millam, J. M., Klene, M., Knox, J. E., Cross, J. B., Bakken, V., Adamo, C., Jaramillo, J., Gomperts, R., Stratmann, R. E., Yazyev, O., Austin, A. J., Cammi, R., Pomelli, C., Ochterski, J. W., Martin, R. L., Morokuma, K., Zakrzewski, V. G.,Voth, G. A., Salvador, P., Dannenberg, J. J., Dapprich, S., Daniels, A.D., Farkas, O., Foresman, J. B., Ortiz, J. V., Cioslowski, J., Fox, D. J. Gaussian. *Inc., Wallingford CT* **2009,** *121*, 150-166.

(7) Henkelman, G.; Jónsson, H. Improved tangent estimate in the nudged elastic band method for finding minimum energy paths and saddle points. *J. Chem. Phys.* **2000,** *113*, 9978-9985.

(8) Zhang, M.; Dou, M.; Yu, Y. DFT study of CO_2 conversion on $InZr_3$ (110) surface. *Phys.Chem.Chem.Phys.* **2017**, *19*, 28917.